ESI for: Is breaking of a hydrogen bond enough to lead to drug resistance?

María José Dávila-Rodríguez[1], Thales Souza Freire[2], Erik Lindahl[3], Ignez Caracelli[2], Julio Zukerman-Schpector[1] and Ran Friedman[3*]

About
This is the Electronic Supplmentary Information

[1] *Federal University of São Carlos, Department of Chemistry, São Carlos-SP, Brazil*
[2] *Federal University of São Carlos, Department of Physics, São Carlos-SP, Brazil*
[3] *Linnæus University, Department of Chemistry and Biomedical Sciences, Kalmar, Sweden*
***Corresponding author**

Contents

1. Methods

1.1 Quantum chemistry

All QM calculations were performed with NWCHEM, version 6.8.1 [1].

1.1.1 Models

The free energy of binding of dasatinib to Abl1 was estimated based on the models presented in Figure S2. The initial coordinates were taken from the crystal structure (PDB id: 2GQG [2]). To make fully-QM calculations feasible, only the part of the protein which is closest to dasatinib is included. Ideally, such a calculation should capture the most important interactions, although it may underestimate the binding free energy since many other interactions are missing. The success of such a model depend on its ability to capture the most important interactions. It is clear that many weak protein-drug interactions are not included, which to some degree is compensated in that the conformation of the complex is strained since the binding residues cannot freely move. Since the X-ray structure was solved for the complex, the stability of the complex is expected to be higher than that of the free protein and drug together. In principle, it is possible to remove this strain by optimising the protein and drug separately. However, especially for the protein this is likely to introduced artefacts since it is not possible to consider all of the protein residues in a fully QM system studied at a high level of accuracy due to computational cost. In addition, in density functional theory (DFT) the interaction of an electron with the entire electron density is included in the coulomb term, leading to the so-called self interaction error (SIE). The exchange-correlation functional should remove this error. Most functionals do not remove all of the SIE [3], which can become severe for large systems [4]. Together, these two effect can paradoxically make a smaller model more accurate than a larger one, as long as such a model indeed captures the essential protein-ligand interactions.

To examine the effect of enlarging the model, the free energy of binding is calculated for three models (Figure S2). The contribution of the hydrogen bond was considered only with the smallest one.

1.1.2 Binding free energy

The structure was optimised in gas phase with the def2-SV(P) basis set [5] and M06 functional [6]. The free energy of binding ΔG^b was then approximated as:

$$\Delta G^b = G_{\text{complex}} - G_{\text{dasatinib}} - G_{\text{protein}} \quad (1)$$

Each of the free energies in Equation 1 was calculated with the def2-TZVP basis set. The solvent (water) was approximated by the SMD solvation model [7]. The M06 functional (hybrid meta-GGA, 27% HF exchange) was used. We report the results in Table S1.

1.1.3 Hydrogen bond energy

The contribution of the hydrogen bond between fragment A and dasatinib to ΔG^b was estimated in the following way.

The distance between fragment A and dasatinib is varied in steps of 0.1 Å. For each distance the interaction energy was calculated with def2-TZVP/M06 and the SMD solvent model. The hydrogen bond energy was then be estimated by

$$\Delta G_{\mathrm{HB}} = \Delta G^{b}_{(d_1)} - \Delta G^{b}_{(d_2)} \tag{2}$$

with $d_1 = 2$ Å and $d_2 = 4.5$ Å.

1.2 Molecular dynamics simulations of Abl1 with dasatinib

MD simulations were carried out using GROMACS [8, 9, 10], version 2018.2. Bonds involving hydrogen atoms were constrained by the LINCS algorithm [11], except for the water molecules for which the SETTLE algorithm [12] was used. The CHARMM36 [13] forcefield was used for the protein. Mutations were introduced with PyMOL, version 1.8 (Schrödinger, LLC).

1.2.1 Model preparation

The structure of the kinase domain of Abl1 bound to dasatinib [2] was downloaded from the protein data bank (PDB id: 2GQG, resolution 2.4 Å). Residue pTyr^{393} (phosphorylated tyrosine) was modelled as tyrosine. All crystallographic waters were removed, to avoid potential bias in the simulations of the mutant proteins or due to the removal of the phosphate group, and as none of the waters is involved in the protein-drug interactions. The complexes of Abl1(T315I) , Abl1(V299L), and Abl1(F317L) with dasatinib were modelled by mutating the corresponding residues in PyMol.

1.2.2 Simulation protocol

The Abl1-dasatinib complex was put in a cubic box extending to al least 1.2 nm from each edge of the protein and solvated by approximately 25000 pre-equilibrated TIP3P water molecules [14]. Potassium and chlorine ions were used to neutralise the system and model a concentration of 0.15 mol L^{-1} to mimic experimental ionic strength conditions. Each system was energy minimised until the maximal force on individual atoms was smaller than 100 KJ mol^{-1} nm^{-1}. Thereafter, a short (20 ps) run was performed with positional restraints on all protein and drug heavy atoms. 40 replicas for each system (Abl1 wt kinase domain, V299L, T315I, F317L) were generated and equilibrated for 5 ns without constraints which led to 40 independent structures in each case. This was followed by 50 ns long production NpT. The temperature (300 K) was kept constant using the velocity rescaling thermostat [15] and the pressure (1 bar) controlled with Berendsen's barostat [16] during position restraint and equilibration simulations, and the Parrinello-Rahman algorithm [17] during production runs. The simulation timestep was 2 fs with van der Waals forces truncated at 1 nm with a plain cutoff and long-range electrostatics treated with the PME method [18, 19]. For wt, V299L and T315I one simulation crashed due to hardware failure and the analysis was based on 39 simulations.

1.2.3 CPU usage

The simulations were carried on the Swedish National Infrastructure for Computations (SNIC) PDC system. For each system, production runs were carried on a system employing an Intel Xeon E5-2698 v3 2.3GHz 16-core - 32-thread processors (ensemble parallelisation, 40 processors in total) which took approximately 49 hours for 50 ns.

1.2.4 Dasatinib parametrisation

Forcefield (CGenFF [20]) parameters for dasatinib were generated using CHARMM-GUI [21, 22]. The parameters were adjusted to ensure planarity of the tiazol and pyrimidine rings with the amine linker. Dasatinib is a base, and it was modelled as a cation with the charge on its distal piperazine nitrogen. Trial simulations were carried out with dasatinib in water to make sure that the compound is structurally stable and does not show any unexpected features. In these simulations, dasatinib's radius of gyration was almost constant (R_g=0.59±0.01 nm) and it was fully solvated forming on average six hydrogen bonds with the water.

1.2.5 Analysis of the simulations

Analysis programs available in GROMACS were used with the default parameters unless otherwise indicated. The number of short contacts between the kinase domain and dasatinib (non-hydrogen atoms) was calculated within a cutoff of 0.4 nm. The free energy landscapes were built using *gmx distance* and *gmx sham* (20 bins per dimension). Interaction energies between dasatinib and the kinase domain correspond to the sum of the average short-range Coulombic interaction energies and the average short-range Lennard-Jones energies obtained with *gmx energy*. The absolute entropy for the bound dasatinib (non-hydrogen atoms) was estimated with the quasi-harmonic approximation [23] after a covariance analysis over all the simulated time of each trajectory using *gmx covar* and *gmx anaeig*. Determination of the configurational entropy of the kinase domain (non-hydrogen atoms residues 240 - 495) was performed as follows. First, cluster analysis was performed employing the algorithm developed by Daura and co-workers [24] with a cutoff of 0.15 nm. The covariance analysis for each trajectory was performed over a patch of five consecutive nanoseconds where the kinase domain was found to be in the same cluster. The entropy was determined based on this covariance analysis according to the quasiharmonic approximation using *gmx anaeig*.

1.3 Free energy perturbation

1.3.1 Theory

Consider the binding of a ligand (L) to a enzyme (E), which can undergo amino acid mutations. To evaluate the binding free energy difference upon this mutation ($\Delta\Delta G^b$) we can

construct a thermodynamic cycle as shown at Eq. 3:

$$\begin{array}{ccc} L+E_{wt} & \xrightarrow{\Delta G^{b}_{wt}} & LE_{wt} \\ \Big\uparrow{\scriptstyle -\Delta G^{apo}_{wt\to mut}} & & \Big\downarrow{\scriptstyle \Delta G^{holo}_{wt\to mut}} \\ L+E_{mut} & \xleftarrow{-\Delta G^{b}_{mut}} & LE_{mut} \end{array} \tag{3}$$

where the *wt* subscript stands for wild type and *mut* for mutated.

As this is a closed cycle it is possible to calculate the desired quantity in two different manners:

$$\Delta\Delta G^{b} = \Delta G^{b}_{mut} - \Delta G^{b}_{wt} \tag{4}$$

$$\Delta\Delta G^{b} = \Delta G^{holo}_{wt\to mut} - \Delta G^{apo}_{wt\to mut} \tag{5}$$

Each approach will need a different simulation setup. For this study the second method (Eq. 5) was used along with Non-equilibrium Statistical Mechanics (NESM) techniques, which required the equilibrium sampling for each state of the enzyme and an ensemble of short transitions between these states in the forward and reverse directions. For each transition the work done by the morphing of one amino acid into another was calculated as:

$$W = \int_0^1 \frac{\partial \mathscr{H}}{\partial \lambda} d\lambda \tag{6}$$

where the Hamiltonian depends on λ as

$$\mathscr{H}(\lambda) = (1-\lambda)\mathscr{H}_{wt} + \lambda \mathscr{H}_{mut} \ , \tag{7}$$

with $\lambda(t=0)=0$ and $\lambda(t=\tau)=1$. λ was increased linearly from 0 to 1 at each time step to perform the complete transition from one equilibrium state to another.

With this work ensemble in hand it is possible to use several methods derived from NESM [25, 26, 27] to calculate $\Delta G^{apo}_{wt\to mut}$ and $\Delta G^{holo}_{wt\to mut}$. For accuracy reasons the Bennet's Acceptance Ratio (BAR) was chosen, as it has an analytical error estimation and a less biased way to calculate the free energy (Eq. 8) than other methods with exponential averaging [28]. Thus, the free energy upon mutation was calculated by solving the following equation:

$$\sum_{i=1}^{N_f} \frac{1}{1+\frac{N_f}{N_r} e^{\beta(W_i-\Delta G)}} = \sum_{j=1}^{N_r} \frac{1}{1+\frac{N_r}{N_f} e^{-\beta(W_j-\Delta G)}} \tag{8}$$

where N_f and N_r are the number of transitions in the forward and reverse direction and $\beta = 1/k_B T$

The convergence of the free energy calculated for the full set of trajectories is determined by the error expression [28]:

$$\frac{1}{\beta^2 N_{tot}} \left[\left\langle \frac{1}{2+2\cosh\left[\beta(W_i-\Delta G)\right]} \right\rangle^{-1} - \left(\frac{N_{tot}}{N_f} + \frac{N_{tot}}{N_r} \right) \right] \tag{9}$$

where the $\langle\rangle$ denotes the average over all work values.

1.3.2 Software and simulation details

MD simulations were performed with GROMACS [8, 9, 10], version 2019.2. The CHARMM36 forcefield [13] was used. , together with the mutation library derived with the pmx program [29]. The TIP3P model [14] was used for water. Bond lengths were constrained by use of the LINCS algorithm [11], except for water molecules, where SETTLE [12] was used instead.

1.3.3 Preparation Stage

The structure of Abl1 bound to dasatinib [2] was downloaded from the protein data bank (PDB id: 2GQG). Crystallographic waters were removed. The GROMACS module *pdb2gmx* was used to build the topology for the kinase domain of the protein. Three mutations (V299L, T315I and F317L) were generated with the *pmx mutate* module of the pmx software [29]. Hybrid topologies, containing information about the wt and the mutated state of the enzyme, were built from these three pdb files, with the *pmx gentop* module . The system was simulated as dodecahedron box, with the enzyme at the centre at 1.2 nm from each side of the box. Then, the system was solvated and K^+ and Cl^- ions were used to neutralise the charges and reach the concentration of 0.15 mM.

1.3.4 Energy minimisation and equilibration

For each mutation a single energy minimisation was performed using a steepest descent algorithm followed by a short MD simulation of 20 ps, where positional restraint were imposed on all protein atoms in order to equilibrate the water molecules around the protein. Next, the system was equilibrated for 5 ns after removing the restraints. The equilibration was repeated ten times for each state of the enzyme to ensure better accuracy through sampling. During the simulations, the Berendsen barostat [16] and velocity rescaling thermostat [15] were used to keep the pressure and temperature constant at 1 bar (with $\tau_p = 1$ ps) and 300 K (with $\tau_t = 0.1$ ps), respectively

1.3.5 Transitions

One hundred snapshots were extracted from each equilibration trajectory. From each of this snapshots, a single short MD simulation of 80 ps was spawned, starting from the wt (forward transition) and from the mutant (reverse transition). This resulted in simulations of 100 transitions in each direction. The Parrinello-Rahman barostat [17] was used for these

simulations, and velocities were generated at each transition run. The Gromacs function *gmx mdrun -dhdl* was used to calculate the change in the Hamiltonian for each simulation step, where the integral along the whole path is the work done at that specific run (Eq 6). Finally, the average free energy for each mutation was obtained with Bennett Acceptance Ratio [27]) using the *pmx analyse* module over all values and averaging over the ten simulations.

1.3.6 CPU usage

The simulations were carried on the SNIC Lunarc system. Each run (equilibration of each state plus 100 forward and 100 reverse transitions) required 45 hours on 10 nodes, each equipped with 2 Intel Xeon E5-2650 v3 (2.3 GHz, 10-core).

1.4 Non-covalent interaction plots

Non-covalent interaction plot (NCIplot) analysis was used in the present study in order to confirm the nature of some of the intermolecular contacts. This method is based on the electron density and its derivatives allowing the visualisation of density gradient isosurfaces. The isosurfaces correspond to the values of sign $(\lambda_2)\rho$, where ρ is the electron density and λ_2 is the second eigenvalue of the Hessian matrix of ρ [30]. This analysis provides a convenient visualisation of the strength of any existing non-covalent interactions through a colour scheme [31] on the isosurface. Here, the viridis colour palette was used, where the gradient colour is changed gradually from purple to blue, green and finally yellow. Thus, purple tones indicate strong attractive interactions (the value of sign$(\lambda_2)\rho$ at low-density gradients is negative). Green surfaces indicate weak interactions (the value of sign$(\lambda_2)\rho$ at low-density gradients is close to zero), whereas yellow coloured surfaces are indicate of strong repulsive interactions (the value of sign$(\lambda_2)\rho$ at low-density gradients is positive).

2. Supplemental Tables

Table S1. The free energy of binding (kcal mol^{-1}) between dasatinib and Abl1 calculated with full QM using three different models (Figure S2) with the def2-TVZP basis set. The rightmost column is the signed error (positive values indicate overbinding by the calculation).

	ΔG^b	error
model 1, 4 residues	−13.3	−1.2
model 2, 5 residues	−15.8	+1.4
model 3, 8 residues	−23.6	+9.2

Table S2. Interaction energies between dasatinib and specific Abl1 residues (kcal mol^{-1}). Numbers are averages calculated over 39 (wt, T315I, F317L) or 40 (V299L) separate 50 ns long simulations for each system, with standard deviation (last significant digit) in parentheses.

Res.		wt		V299L		T315I		F317L
299	V	−1.3(02)	**L**	−1.5(02)	V	−0.6(04)	V	−1.3(02)
315	T	−6.7(07)	T	−5.9(2)	**I**	−2.6(1)	T	−6.7(06)
317	F	−5.5(04)	F	−5.5(06)	F	−5.9(04)	**L**	−3.4(02)
318	M	−11.7(04)	M	−11.6(04)	M	−11.7(03)	M	−12.0(04)
All		−72.4(7)		−70.3(8)		−61.7(6)		−72.8(7)
$\Delta\Delta E^b$				2.1		10.7		−0.3

3. Supplemental Figures

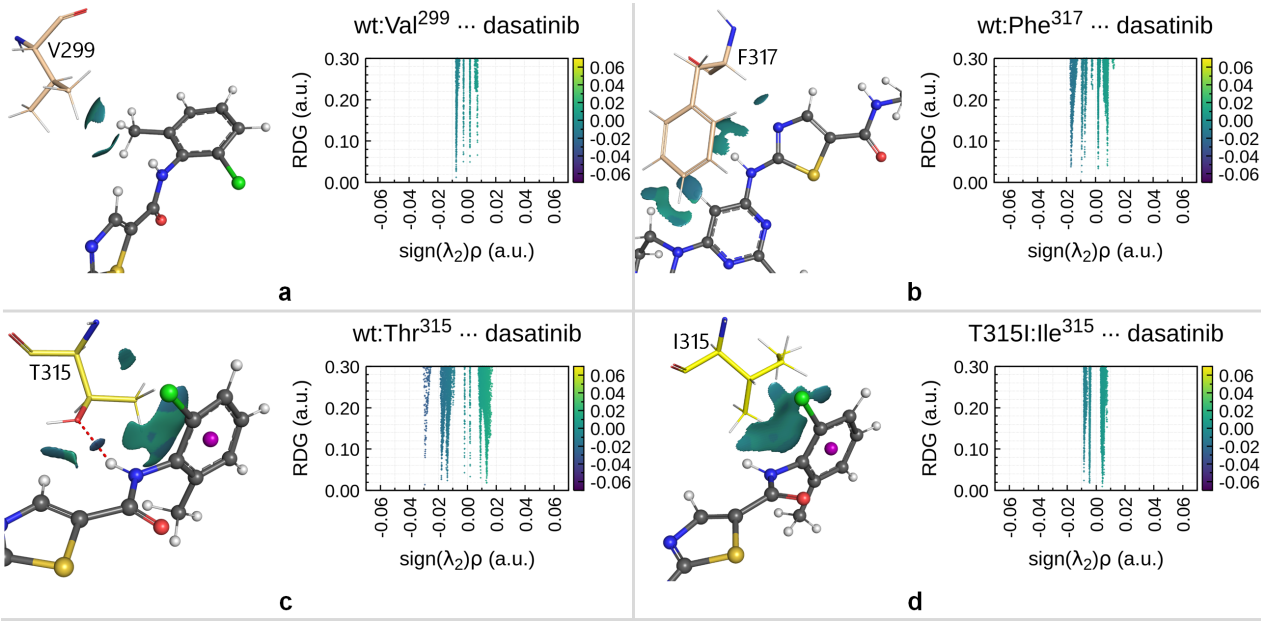

Figure S1. NCI analysis. Isosurfaces representing non-covalent interactions are presented and coloured according to $\mathrm{sign}(\lambda_2)\rho$ on the left side of which panel, whereas plots of reduced density gradient, RDG, versus $\mathrm{sign}(\lambda_2)\rho(r)$ are shown on the right. NCI plots are shown for dasatinib and (a) Val^{299} (b) Phe^{317} (c) Thr^{315}, (d) Ile^{315} in the T315I mutant. NCI plots are calculated based on an equilibrated structure from an MD simulation in each case. Protein figures were created with PyMOL.

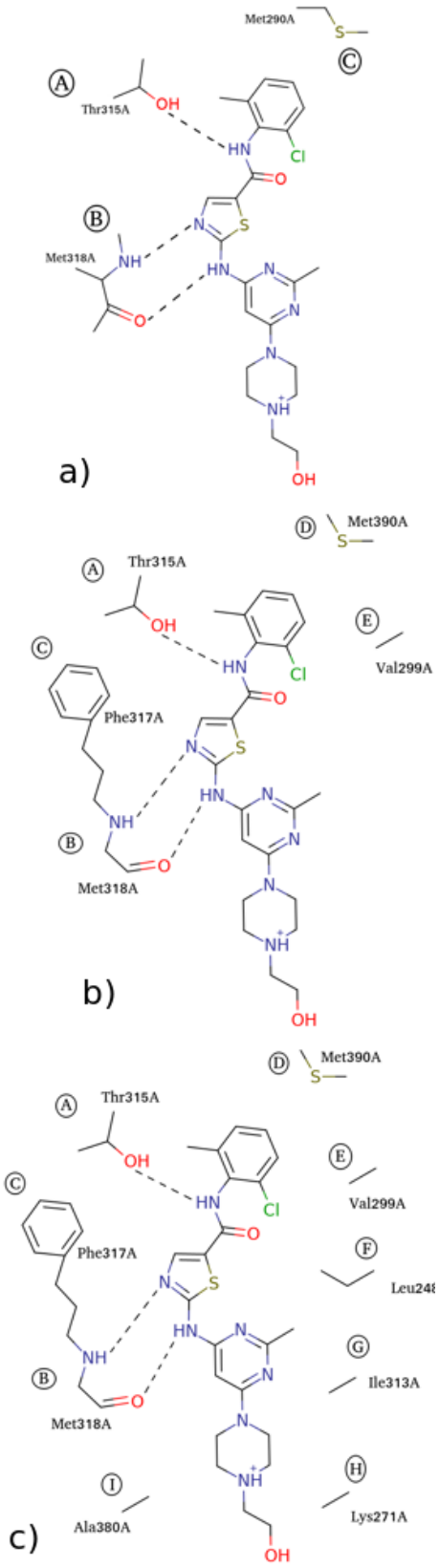

Figure S2. Models used to calculate the free energy of interaction between dasatinib and Abl1. Dotted lines indicate hydrogen bonds. a) The original (minimal) model, model 1. b) Model 2. c) Model 3.

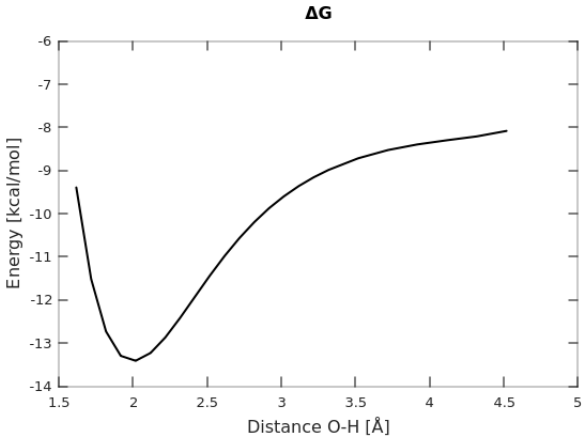

Figure S3. Interaction free energy for dasatinib's binding to Abl1, as a function of the T315:OH–NH:dasatinib hydrogen bond distance.

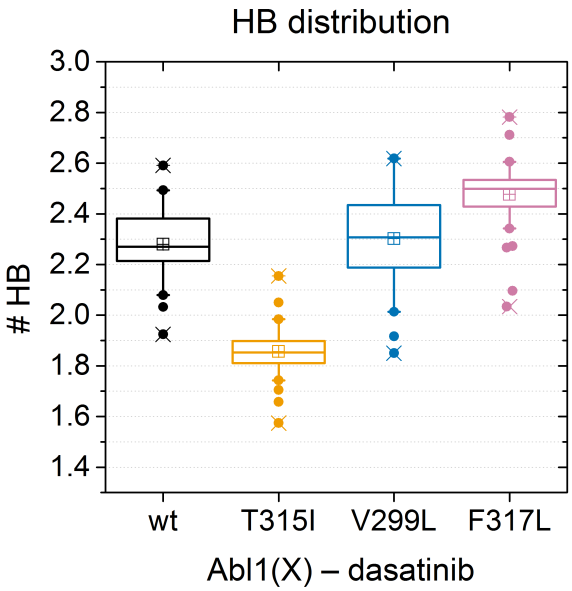

Figure S4. Distribution of the hydrogen bonds between Abl1 and dasatinib for the wt and mutants (box plot).

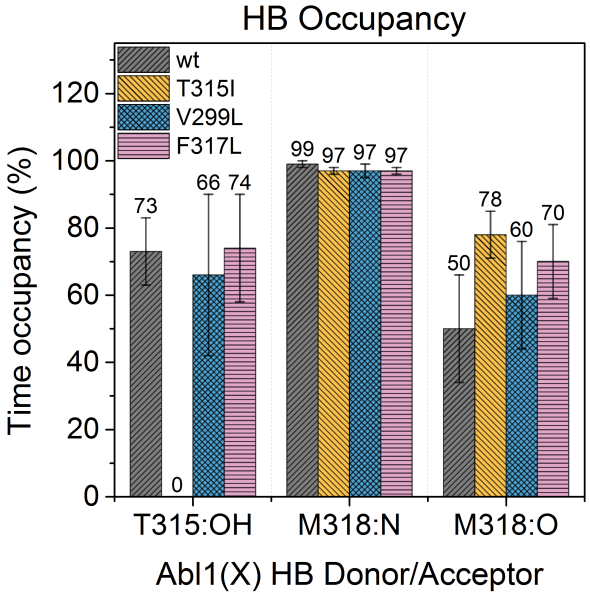

Figure S5. Hydrogen bond occupancies during the simulations.

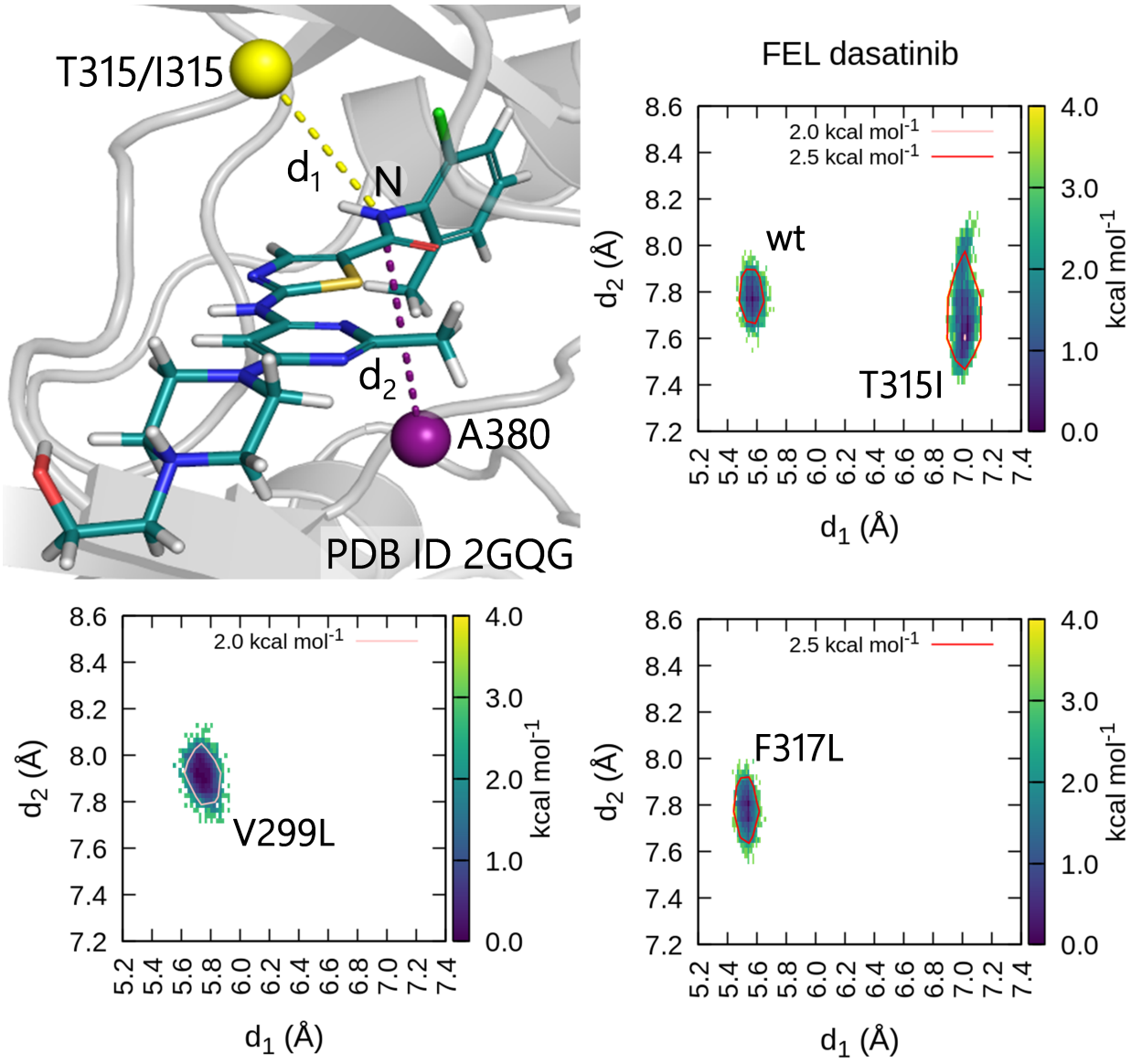

Figure S6. Two dimensional free energy landscapes calculated as a function of the two distances d_1 and d_2 monitored for the four different simulations. d_1 is the distance to the centre of mass (COM) of the backbone of the gatekeeper residue. d_2 is the distance to the COM of the backbone of residue Ala^{380} which precedes the DFG motif and activation loop.

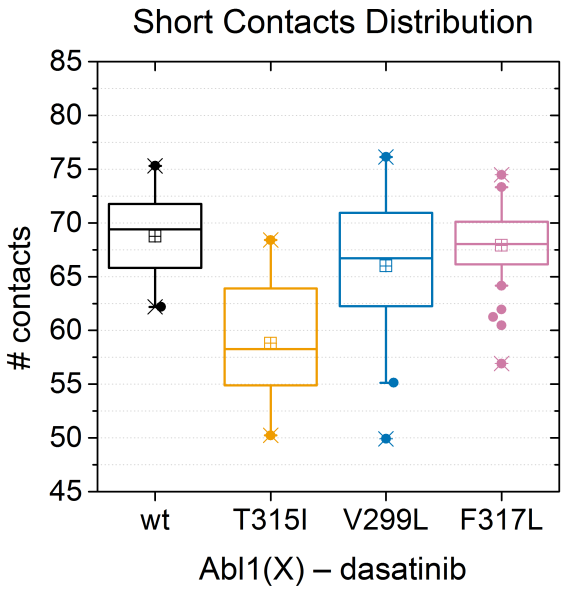

Figure S7. Distribution of the number of contacts (d<4Å) between Abl1 and dasatinib for the wt and mutants (box plot).

References

[1] M. Valiev, E.J. Bylaska, N. Govind, K. Kowalski, T.P. Straatsma, H.J.J. Van Dam, D. Wang, J. Nieplocha, E. Apra, T.L. Windus, and W.A. de Jong. Nwchem: A comprehensive and scalable open-source solution for large scale molecular simulations. *Comput. Phys. Commun.*, 181(9):1477 – 1489, 2010.

[2] J S Tokarski, J A Newitt, C Y Chang, J D Cheng, M Wittekind, S E Kiefer, K Kish, F Y Lee, R Borzillerri, L J Lombardo, D Xie, Y Zhang, and H E Klei. The structure of Dasatinib (BMS-354825) bound to activated ABL kinase domain elucidates its inhibitory activity against imatinib-resistant ABL mutants. *Cancer Res*, 66:5790–5797, 2006.

[3] J. L. Bao, L. Gagliardi, and D. G. Truhlar. Self-Interaction Error in Density Functional Theory: An Appraisal. *J Phys Chem Lett*, 9(9):2353–2358, May 2018.

[4] Adam Fouda and Ulf Ryde. Does the dft self-interaction error affect energies calculated in proteins with large qm systems? *J. Chem. Theor. Comput.*, 12:5667–5679, 2016.

[5] F Weigend and R Ahlrichs. Balanced basis sets of split valence, triple zeta valence and quadruple zeta valence quality for H to Rn: Design and assessment of accuracy. *Phys. Chem. Chem. Phys.*, 7:3297–3305, 2005.

[6] Y Zhao and D G Truhlar. The M06 suite of density functionals for main group thermochemistry, thermochemical kinetics, noncovalent interactions, excited states, and transition elements: Two new functionals and systematic testing of four m06 functionals and twelve other functionals. *Theor. Chem. Acc.*, 120:215–214, 2008.

[7] A. V. Marenich, C. J. Cramer, and D. G. Truhlar. Universal solvation model based on solute electron density and on a continuum model of the solvent defined by the bulk dielectric constant and atomic surface tensions. *J Phys Chem B*, 113(18):6378–6396, May 2009.

[8] H. J. C. Berendsen, D. van der Spoel, and R. Vandrunen. Gromacs - a message-passing parallel molecular-dynamics implementation. *Comput. Phys. Commun.*, 91:43–56, 1995.

[9] D. van der Spoel, E. Lindahl, B. Hess, G. Groenhof, A. E. Mark, and H. J. C. Berendsen. Gromacs: Fast, flexible, and free. *J. Comput. Chem.*, 26:1701–1718, 2005.

[10] Mark James Abraham, Teemu Murtola, Roland Schulz, Szilárd Páll, Jeremy C. Smith, Berk Hess, and Erik Lindahl. GROMACS: High performance molecular simulations through multi-level parallelism from laptops to supercomputers. *SoftwareX*, 1–2:19–25, 2015.

[11] B. Hess, H. Bekker, H. J. C. Berendsen, and J. G. E. M. Fraaije. LINCS: A linear constraint solver for molecular simulations. *J. Comp. Chem.*, 18:1463–72, 1997.

[12] S. Miyamoto and P. A. Kollman. SETTLE: An analytical version of the SHAKE and RATTLE algorithms for rigid water models. *J. Comp. Chem.*, 13:952–962, 1992.

[13] R. B. Best, X. Zhu, J. Shim, P. E. Lopes, J. Mittal, M. Feig, and A. D. Mackerell. Optimization of the additive CHARMM all-atom protein force field targeting improved sampling of the backbone ϕ, ψ and side-chain χ_1 and χ_1 dihedral angles. *J Chem Theory Comput*, 8(9):3257–3273, Sep 2012.

[14] W. L. Jorgensen, J. Chandrasekhar, J. D. Madura, R. W. Impey, and M. L. Klein. Comparison of simple potential functions for simulating liquid water. *J. Chem. Phys.*, 79:926–935, 1983.

[15] G Bussi, D Donadio, and M Parrinello. Canonical sampling through velocity rescaling. *J Chem Phys*, 126:014101, 2007.

[16] H. J. C. Berendsen, J. P. M. Postma, A. DiNola, and J. R. Haak. Molecular dynamics with coupling to an external bath. *J. Chem. Phys.*, 81:3684–90, 1984.

[17] M. Parrinello and A. Rahman. Polymorphic transitions in single crystals: A new molecular dynamics method. *J. Appl. Phys.*, 52:7182–7190, 1981.

[18] T. Darden, D. York, and L. Pedersen. Particle mesh ewald: An N-log(N) method for ewald sums in large systems. *J. Chem. Phys.*, 98:10089–92, 1993.

[19] Ulrich Essmann, Lalith Perera, Max L. Berkowitz, Tom Darden, Hsing Lee, and Lee G. Pedersen. A smooth particle mesh ewald method. *J. Chem. Phys.*, 103(19):8577–8593, 1995.

[20] K. Vanommeslaeghe, E. Hatcher, C. Acharya, S. Kundu, S. Zhong, J. Shim, E. Darian, O. Guvench, P. Lopes, I. Vorobyov, and A. D. Mackerell. Charmm general force field: A force field for drug-like molecules compatible with the charmm all-atom additive biological force fields. *J. Comput. Chem.*, 31(4):671–690, 2010.

[21] S. Jo, M. Vargyas, J. Vasko-Szedlar, B. Roux, and W. Im. PBEQ-Solver for online visualization of electrostatic potential of biomolecules. *Nucleic Acids Res.*, 36(Web Server issue):W270–275, Jul 2008.

[22] S. Kim, J. Lee, S. Jo, C. L. Brooks, H. S. Lee, and W. Im. CHARMM-GUI ligand reader and modeler for CHARMM force field generation of small molecules. *J Comput Chem*, 38(21):1879–1886, 06 2017.

[23] I. Andricioaei and M. Karplus. On the calculation of entropy from covariance matrices of the atomic fluctuations. *J. Chem. Phys.*, 115:6289–6292, 2001.

[24] Xavier Daura, Karl Gademann, Bernhard Jaun, Dieter Seebach, Wilfred F. van Gunsteren, and Alan E. Mark. Peptide folding: When simulation meets experiment. *Angew. Chem. Int. Ed.*, 38:236–240, 1999.

[25] Gavin E. Crooks. Entropy production fluctuation theorem and the nonequilibrium work relation for free energy differences. *Phys. Rev. E*, 60(3):2721–2726, Jan 1999.

[26] C. Jarzynski. Nonequilibrium equality for free energy differences. *Phys. Rev. Lett.*, 78(14):2690–2693, Jul 1997.

[27] Charles H Bennett. Efficient estimation of free energy differences from monte carlo data. *J. Computat. Phys.*, 22(2):245–268, 1976.

[28] Michael R. Shirts, Eric Bair, Giles Hooker, and Vijay S. Pande. Equilibrium free energies from nonequilibrium measurements using maximum-likelihood methods. *Phys. Rev. Lett.*, 91(14), Feb 2003.

[29] V. Gapsys, S. Michielssens, D. Seeliger, and B. L. de Groot. pmx: Automated protein structure and topology generation for alchemical perturbations. *J Comput Chem*, 36(5):348–354, Feb 2015.

[30] E. R. Johnson, S. Keinan, P. Mori-Sánchez, J. Contreras-Garc?a, A. J. Cohen, and W. Yang. Revealing noncovalent interactions. *J. Am. Chem. Soc.*, 132(18):6498–6506, May 2010.

[31] J. Contreras-García, E. R. Johnson, S. Keinan, R. Chaudret, J. P. Piquemal, D. N. Beratan, and W. Yang. NCIPLOT: a program for plotting non-covalent interaction regions. *J Chem Theory Comput*, 7(3):625–632, Mar 2011.